Phase diagram for amorphous solid water

Peter H. Poole,[1,2] Ulrich Essmann,[1,*] Francesco Sciortino,[1,3] and H. Eugene Stanley[1]
[1]*Center for Polymer Studies and Physics Department, Boston University, Boston, Massachusetts 02215*
[2]*Department of Chemistry, Arizona State University, Tempe, Arizona 85287*
[3]*Dipartimento di Fisica, Universitá "La Sapienza," Piazzale Aldo Moro, 00185 Roma, Italy*
(Received 16 August 1993)

We show how the observed transformation behavior of two forms of amorphous solid water can be explained in terms of a first-order phase transition, via a consideration of the limits of metastability associated with this kind of transition. We propose a phase diagram describing amorphous solid water consistent with the available experimental data. We support this phase diagram with thermodynamic and structural results of computer simulations using two distinct water interaction potentials, specifically the ST2 potential of Stillinger and Rahman [J. Chem. Phys. **60**, 1545 (1974)] and the TIP4P potential of Jorgensen *et al.* [J. Chem. Phys. **79**, 926 (1983)].

PACS number(s): 64.70.Kb, 61.43.Bn, 64.30.+t, 64.70.Ja

Considerable recent interest has focused on the study of the amorphous solid form of water, "amorphous ice." This has occurred for several reasons. (i) Amorphous ice is the glass state of an especially common substance, and so has importance in a variety of fields such as astrophysics [1] and cryobiology [2]. (ii) The properties of liquid water in its supercooled state, which appears during hyperquenching to amorphous ice, are matters of on-going scientific debate [3]. (iii) The structure of the amorphous *solid* has been proposed as a model for the structure of the *liquid* in order to elucidate the puzzling behavior of liquid water [4]. (iv) A particularly striking feature of amorphous ice is that at least two distinct amorphous forms are observed to occur [5–14], an experimental fact that is not fully understood.

The two observed forms of amorphous ice differ significantly in their density and their microscopic structure. One form, low-density amorphous ice (LDA ice), can be formed by vapor deposition at a temperature T below 77 K [5], or by hyperquenching of the liquid directly to an amorphous solid [6–8,12–14]. The other observed form, high-density amorphous ice (HDA ice) can be produced through pressure-induced amorphization of ice I_h at 77 K [9]. Also, if LDA ice is isothermally compressed at 77 K, it transforms at a pressure $P \sim 600$ MPa to HDA ice [10]. HDA ice can be recovered at $P = 1$ atm, and further, is observed to transform to LDA ice when warmed above $\sim$ 120 K [10]; this phenomenon thus provides another method for generating LDA ice. HDA ice at $P = 1$ atm has a significantly higher density ($\rho = 1.17$ g/cm^3) than LDA ice ($\rho = 0.94$ g/cm^3). It has been suggested, from the abrupt character of the pressure-induced LDA→HDA ice transition, that a first-order phase transition separates these two amorphous forms [10,15–19].

Beyond the observation that the transformation of LDA to HDA ice *appears* to be a first-order phase transition, there is little understanding of the thermodynamic relationship between these two forms of amorphous ice (see, however, Ref. [20]). There also exist important questions concerning the thermodynamic relationship of the amorphous ices to both the liquid just above the glass transition temperature and to the liquid above the melting temperature [14,21,22].

Here we propose a specific phase diagram relating LDA and HDA ice, and show that this phase diagram is consistent with available experimental data. Further, we support the proposed phase diagram through molecular dynamics (MD) computer simulations of amorphous ice.

The phase diagram we propose [see Fig. 1(a)] postulates the existence of a line of first-order phase transitions that separates LDA and HDA ice. We find that the properties of amorphous ice can be understood through a consideration of the behavior of the limits of metastability—or spinodals—that are commonly associated with such a first-order phase-transition line ending in a critical point [23]. These two spinodal lines, denoted by L and H in Fig. 1(a), define the absolute limits of thermal and mechanical stability for the two phases. The line L is the metastability limit for LDA ice, while H defines the metastability limit for HDA ice. Hence, LDA ice is the more stable amorphous solid below the first-order transition line F, yet may also be observed in the region above F but below L, where it is metastable with respect to HDA ice. Above L, LDA ice becomes unstable. Similarly, HDA ice is the more stable form above F, is metastable with respect to LDA ice between F and H, and is unstable below H.

Note that L and H necessarily delineate metastable equilibrium states, in the sense that all amorphous states in the temperature range shown are metastable with respect to the formation of crystalline ice. However, the low molecular mobility at these temperatures can suppress the modes of structural relaxation that are required for the formation of the crystal within practical observation times. Furthermore, this same low mobility also precludes the amorphous system from completely relaxing into a true metastable equilibrium state, like that of a supercooled liquid. Under these glassy conditions, the characteristic relaxation times of the system greatly exceed the time scale of the observations. Such a system

*Present address: Department of Chemistry, University of North Carolina, Chapel Hill, NC 27599.

is subject to nonequilibrium kinetic effects which cause its properties to vary as a function of how the system is brought to a given state. Therefore, we expect that in real experiments, as well as in MD simulations, any transitions observed in practice may be strongly shifted from the "ideal" equilibrium locations proposed in Fig. 1(a). The extent to which this shift appears in our MD simulation results (described below) is shown in Fig. 1(b). In spite of this difficulty, we show in the following that the metastable equilibrium behavior shown in Fig. 1(a) offers a useful framework for understanding experimental and simulation results, even though these results are obtained from a system which has not completely reached equilibrium.

Figures 1(c) and 1(d) respectively show the regions of the phase diagram where LDA ice and HDA ice may be observed as metastable states. With these plots, we can show how the phase diagram of Fig. 1(a) accounts for experimental observations.

(i) At low T and $P = 1$ atm, both forms of amorphous ice are observed [9,10]: LDA ice, which is metastable with respect to the crystal; and HDA ice, which is metastable with respect to both LDA ice and the crystal. This is possible because the region near $P = 1$ atm for $T < 120$ K lies *between* the spinodals L and H, where both LDA and HDA ice are metastable states. The phase observed will thus depend on the thermodynamic path taken by the experimental preparation procedure, as discussed in the following.

(ii) Hyperquenching of the liquid at $P = 1$ atm [6] will produce LDA ice [path a in Fig. 1(c)], because the region of the phase diagram in which LDA ice is metastable is continuously connected at this P to the region of the liquid state by a path which does not intersect either the coexistence line F or the LDA→HDA ice spinodal L.

(iii) Isothermal compression of LDA ice at 77 K [10] to P greater than that of the LDA→HDA spinodal L will induce the transition to HDA ice [path b in Fig 1(c)].

(iv) If pressure is removed from HDA ice at 77 K, HDA ice can be observed [10] as a metastable state at $P = 1$ atm [path c in Fig. 1(d)], because it does not cross the HDA→LDA ice spinodal H.

(v) The observability of HDA ice at $P = 1$ atm is limited by the location of the HDA→LDA ice spinodal H. Thus, when the temperature of HDA ice exceeds the temperature of the line H at $P = 1$ atm, it transforms to

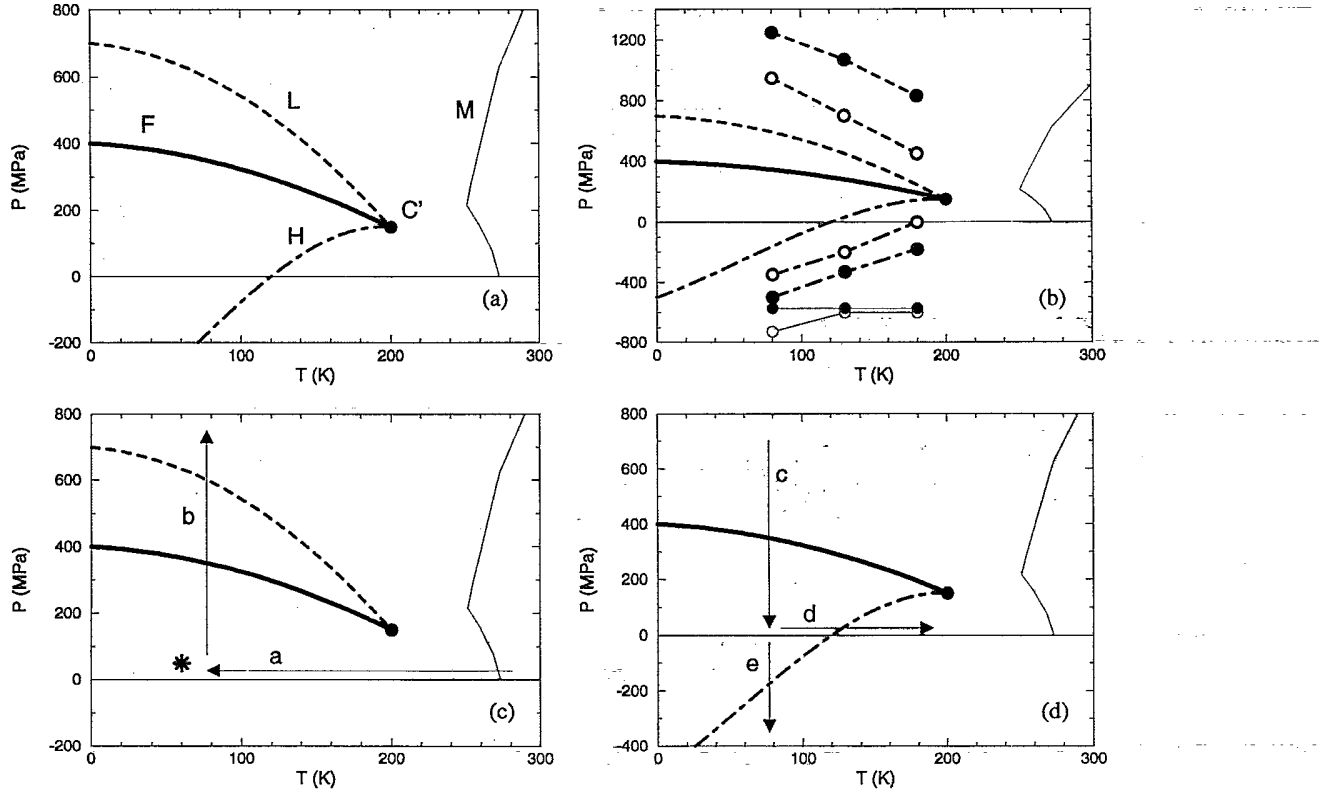

FIG. 1. (a) Proposed P-T phase diagram for amorphous solid water. Above the first-order phase transition line F, HDA ice is the more stable amorphous solid; LDA ice is the more stable phase below F. The HDA→LDA spinodal (H) and the LDA→HDA spinodal (L) meet at the critical point C'. M is the equilibrium melting line of crystalline ice. (b) Comparison of the features given in a and those estimated from the present MD simulations. Results for ST2 are indicated by (•) and for TIP4P by (o). Dashed lines denote the LDA→HDA transitions, while dot-dashed lines indicate the HDA→LDA transitions. Also shown are the pressures of fracture observed in the simulations (symbols connected by thin solid lines). (c) The thermodynamic features from a that determine the region of observability of LDA ice. Path a represents the quenching of LDA ice from the liquid. Along path b, LDA ice passes beyond its limit of metastability (L) and converts to HDA ice. The point indicated by (*) represents a vapor deposition experiment. (d) The thermodynamic features from a that determine the region of observability of HDA ice. Along path c, HDA ice is recovered at $P = 1$ atm, while along paths d (warming) or e (stretching), HDA ice passes beyond its limit of metastability (H) and converts to LDA ice.

LDA ice [path d in Fig. 1(d)], as observed in experiments [10].

(vi) Since vapor deposition [denoted by $*$ in Fig. 1(c)] is not a process that corresponds to a thermodynamic path, it can produce either phase, depending on the temperature and the deposition rate. Since LDA ice is more stable than HDA ice at $P = 1$ atm we expect that the LDA ice will be preferred at higher T and slower deposition rate, as observed in experiments [16,17].

To support the proposed phase diagram, we have used MD simulations [24–26] to map out the region of mechanical stability of both HDA and LDA ice phases. The utility of the MD approach is supported by calculations on the pressure-induced transition of crystalline ice I_h to HDA ice [27]. We have carried out parallel analyses using both the ST2 [28] and TIP4P [29] pair potentials to confirm that our conclusions are not artifacts of the interparticle potential. We first prepare a configuration of molecules analogous to LDA ice by computationally quenching an equilibrated liquid state configuration [30]. We then subject this simulated LDA ice system to isothermal compression at a fixed rate of pressure increase up to ~ 1800 MPa, at different T [31].

The response of ρ to the applied P is shown in Fig. 2 for ST2 (top panel) and TIP4P (bottom panel). Although initially all isotherms indicate that the compression of the amorphous solid is small, each exhibits a well-defined region in P around a critical value P_L in which ρ increases dramatically. For $P > P_L$, the response of ρ suggests a return to low compressibility. In general, the transition of the amorphous solid in the region of P_L is reminiscent of the LDA→HDA ice transition observed in isothermal compression experiments at 77 K [10]. In the case of the ST2 system, the collapse is quite abrupt and is associated for all T with a density jump from $\rho \sim 0.95$ g/cm^3 to $\rho \sim 1.45$ g/cm^3. The transition in the TIP4P system, however is less abrupt: the density changes only from $\rho \sim 1.0$ g/cm^3 to $\rho \sim 1.3$ g/cm^3. TIP4P reproduces the experimental value $\rho = 1.31$ g/cm^3 [10] for the density of HDA ice above the transition pressure P_L better than ST2.

Decreasing the pressure to $P = 0$ MPa, at the same rate, leads in both ST2 and TIP4P to a decrease in ρ. The TIP4P system compares well with the experimental behavior. We find that at $T = 80$ K, ρ for TIP4P decreases from 1.34 g/cm^3 to 1.21 g/cm^3, close to the experimental value $\rho = 1.17$ g/cm^3 found at $T = 77$ K [10]. Continued decompression into the region of negative P, where the system is subject to a hydrostatic tensile stress, inevitably induces fracture of the amorphous solid.

The ST2 simulations show that fracture occurs at all three temperatures near $P = -550$ MPa and $\rho \sim 0.72$ g/cm^3. Notably, however, the decompression isotherms at $T = 130$ and 180 K display a region around a critical value P_H prior to complete fracture in which an abrupt change of the density is observed that does not lead to fracture, but to the formation of a lower-density substance which is then itself stretched to its tensile limit. The density of the system after this change is consistent with a transformation to a stretched LDA ice, which is stable at $T = 180$ K against the applied tension over a range of more than 300 MPa before fracture is finally observed. At lower $T = 130$ K, the transformation to LDA ice occurs at a lower value of P_H. At $T = 80$ K the transition occurs at the same P as the fracture and so is undistinguishable from it.

The TIP4P system shows similar features. The simulations indicate that for all temperatures fracture occurs near the same density of $\rho \sim 0.84$ g/cm^3. However, the P at which the system fractures increases as T increases. Also, prior to the fracture, a feature similar to that found in the ST2 simulations appears which suggests that first a transition from HDA to LDA ice occurs, as indicated by a strong decrease in density to about $\rho \sim 0.95$ g/cm^3. As in the ST2 system, the pressure P_H of this transition in TIP4P shifts to higher values as T increases.

Next we interpret the simulation results of Fig. 2 in terms of our proposed phase diagram. Initially the LDA ice system is progressively compressed until the limit of

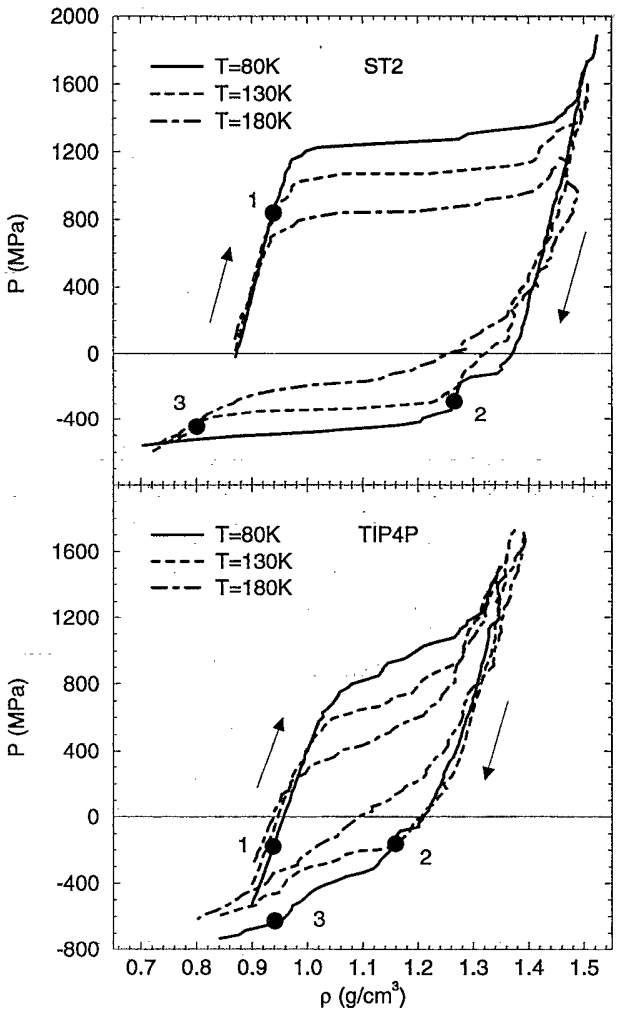

FIG. 2. Response of the density ρ during isothermal compression (up arrows) and decompression (down arrows) of amorphous solid water simulated with ST2 (top panel) and TIP4P (bottom panel), at several different T. The systems fracture at the points of lowest P and ρ shown along the decompression paths. The numbered points (•) identify the states for which the structure is given in Fig. 3.

metastability of the LDA phase L is reached [path b in Fig.1(c)]. At this point, at $P = P_L$, the system converts to the HDA phase; on further increase of P the HDA phase itself is compressed. On decreasing P, the HDA system converts to LDA ice at a much lower $P = P_H$, corresponding to the HDA→LDA limit of metastability H being reached [path e in Fig.1(d)]. Note that the transitions are therefore not observed (either in experiments or in simulations) along the equilibrium coexistence line F between the two amorphous phases, but rather at the metastability limits identified above. The fluctuations required to nucleate the equilibrium phase transition at the coexistence line F do not exist in this low-T glassy regime. The transitions therefore only occur at the metastability limits L and H, where the onset of intrinsic thermodynamic instability within a given phase can prompt the transformation. Our estimate for the position of F in Fig. 1 is thus speculative, and should not be considered quantitatively correct.

The temperature dependence of the values of P_L and P_H are shown in Fig. 1(b) for both ST2 and TIP4P. We note that as T increases, the LDA→HDA transition shifts to lower P, whereas the HDA→LDA transition shifts to higher P. Taking the respective values of P_L and P_H as estimates for the positions of the spinodal lines L and H, we find that L and H approach each other. This behavior is consistent with the recent conjecture [32,33] that the first-order phase transition line F terminates in a critical point [C' in Fig. 1(a)] at which an intersection of spinodal lines may be expected. The possibility that F terminates at C' implies that at sufficiently high T LDA and HDA ice become indistinguishable. This possibility, that the transition can be found to be either discontinuous or continuous, is consistent with the fact that both phases are amorphous solids.

We also find that the phase diagram in Fig. 1(a) is supported by a comparison of the structure of the simulated amorphous solid to that of LDA and HDA ice [19,34–37]. In Fig. 3 we compare the weighted pair-correlation function $h(r)$, as measured in neutron scattering experiments on amorphous solid water, and as calculated in the present simulations [38]. We see that the configurations at the beginning of the compression runs have a structure similar to that of the LDA ice (top panels). The $h(r)$ after the initial decompression (middle panels) compares well with the structure of HDA ice, especially in the case of TIP4P. Further, the systems recovered at negative P and low ρ (bottom panels) have returned to a structure similar to that at the beginning of their respective compression runs, and also similar to the LDA ice structure. This last observation supports the suggestion, implicit in our proposed phase diagram, that HDA ice is able to transform back to LDA ice at sufficiently low P, but before fracture.

For both ST2 and TIP4P, the $h(r)$ function before and after the compression-decompression cycle is similar, suggesting that the system returns after sufficient decompression to the initial state. However, we observe that the compressibility, as may be derived from the slope of the P versus ρ plots in Fig. 2, has changed. Also, there is a difference in the total potential energy U before and after the cycle, typically of about 1.5 kJ/mol. We associate such differences with the lack of complete relaxation to equilibrium in our simulations: the low T does not allow for a complete rearrangement of the local molecular configurations during decompression, a fact that is not so strongly indicated by the $h(r)$ function as it is by U. To confirm this interpretation we anneal at $T = 130$ K a TIP4P configuration with $\rho = 0.975$ g/cm^3 produced during the $T = 130$ K decompression run. After annealing at constant ρ for 500 ps, we observe indeed that U relaxes about 50% of the way to the value of U observed at this ρ during the initial compression run. Longer simulations, unfeasible at the present time, would be necessary to completely clarify this point.

To summarize, we have shown that it is possible to construct a phase diagram using only concepts of metastable equilibrium thermodynamics, which accounts for the observed transformation behavior of amorphous solid water. However, this is not to say that experimental observations, or indeed, the MD simulation results, are not consistent with other interpretations. In particular, the influence of nonequilibrium kinetic phenomena must be studied more systematically than we attempt here be-

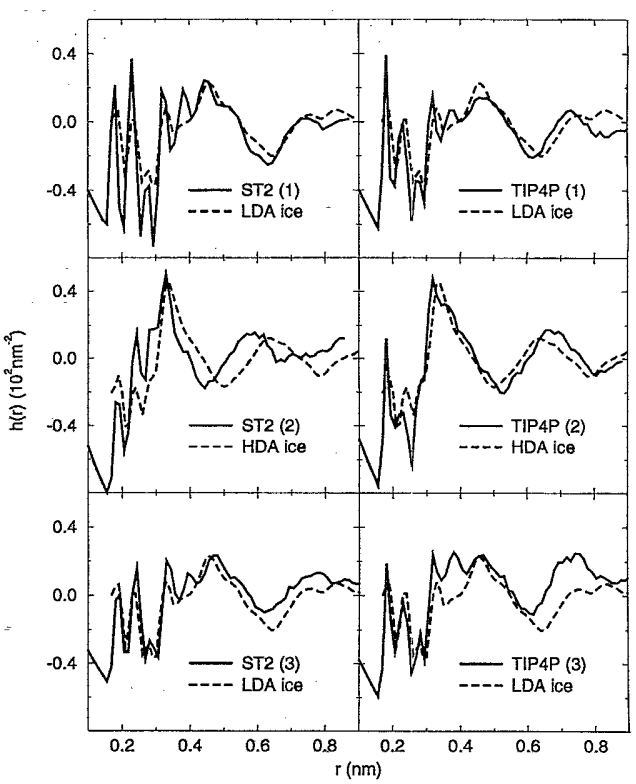

FIG. 3. The $h(r)$ function calculated during the ST2 and TIP4P compression-decompression cycles shown in Fig. 2, compared with the experimental $h(r)$ for LDA and HDA ice. The numbers in parentheses labeling the simulation data correspond to the numbered points in Fig. 2: thus the structures of the systems at the beginning of the compression (top pair of panels), after decompression (middle panels), and just prior to fracture (bottom panels), are shown. All the simulated structures are derived from the $T = 80$ K runs, with the single exception of the "ST2(3)" curve, which was taken from the $T = 130$ K simulation.

fore a definitive understanding will be possible. Yet the present analysis, which deliberately neglects nonequilibrium effects, yields a result which is both internally consistent and consistent with observation. Our results therefore confirm the possibility that thermodynamic phenomena, such as a first-order phase transition and spinodal metastability limits, play a significant role in the transformations of amorphous solid water.

Before concluding, we further note that from the phase diagram of Fig. 1(a) follow specific predictions which can be tested experimentally: within the regime where crystallization does not preclude the observation of the amorphous solid phases, (i) the pressure for the LDA→HDA transition should decrease as a function of increasing temperature, and (ii) the observed transition temperature for the HDA → LDA transformation should increase with increasing pressure.

We would like to thank C. A. Angell, T. Grande, M. Hemmati, P. F. McMillan, S. Sastry, J. Shao, and G. H. Wolf for enlightening discussions. Financial support was provided by BP and NSF.

[1] E. Mayer and R. Pletzer, Nature **319**, 298 (1986).
[2] P. Mazur, Science **168**, 939 (1970).
[3] C. A. Angell, Ann. Rev. Phys. Chem. **34**, 593 (1983); see also Y. Xie, K. F. Ludwig, G. Morales, D. E. Hare, and C. M. Sorensen, Phys. Rev. Lett. **71**, 2050 (1993).
[4] M. G. Sceats and S. A. Rice in *Water: A Comprehensive Treatise*, edited by F. Franks (Plenum, New York, 1982), Vol. 7.
[5] E. F. Burton and W. F. Oliver, Nature **135**, 505 (1935); Proc. R. Soc. London Ser. A **153**, 166 (1935).
[6] P. Brügeller and E. Mayer, Nature **288**, 569 (1980).
[7] J. Dubochet and A. W. McDowall, J. Microscopy **124**, RP3 (1981).
[8] E. Mayer and P. Brüggeller, Nature **298**, 715 (1982).
[9] O. Mishima, L. D. Calvert, and E. Whalley, Nature **310**, 393 (1984).
[10] O. Mishima, L. D. Calvert, and E. Whalley, Nature **314**, 76 (1985).
[11] Y. P. Handa, O. Mishima, and E. Whalley, J. Chem. Phys. **84**, 2766 (1986).
[12] E. Mayer, J. Appl. Phys. **58**, 663 (1985).
[13] G. P. Johari, A. Hallbrucker, and E. Mayer, Nature **330**, 552 (1987).
[14] A. Hallbrucker, E. Mayer, and G. P. Johari, Philos. Mag. B **60**, 179 (1989).
[15] Note that there is some debate concerning whether the low-density amorphous solids formed by different methods actually give the same unique product. For example, the conditions under which vapor deposition is performed affect the properties of the amorphous solid product [16,17]. However, thermal and structural analysis indicates that the methods described in the text for generating a low-density amorphous solid produce the same substance. This fact motivates our grouping of all low-density forms under the common name of "LDA ice" [18,19].
[16] A. H. Narten, C. G. Venkatesh, and S. A. Rice, J. Chem. Phys. **64**, 1106 (1976).
[17] E. Mayer and R. Pletzer, J. Chem. Phys. **80**, 2939 (1984).
[18] A. Hallbrucker, E. Mayer, and G. P. Johari, J. Phys. Chem. **93**, 4986 (1989).
[19] M.-C. Bellissent-Funel, L. Bosio, A. Hallbrucker, E. Mayer, and R. Sridi-Dorbez, J. Chem. Phys. **97**, 1282 (1992).
[20] E. Whalley, D. D. Klug, and Y. P. Handa, Nature **342**, 782 (1989).
[21] R. J. Speedy, J. Phys. Chem. **96**, 2322 (1992).
[22] C. A. Angell, J. Phys. Chem. **97**, 6339 (1993).
[23] J. D. Gunton, M. San Miguel, and P. S. Sahni, in *Phase Transitions and Critical Phenomena*, edited by C. Domb and J. L. Lebowitz (Academic, London, 1983), p. 267.
[24] All the MD simulations reported here consist of a system of 216 water molecules enclosed in a cubic box, using periodic boundary conditions. Interactions between water molecules are explicitly calculated up to a cutoff distance of 0.78 nm for ST2, and 0.7934 nm for TIP4P. The effect of Coulomb forces due to molecules beyond this cutoff distance is treated by a reaction-field method [25]. The time step for the integration of the molecular trajectories is fixed at 1 fs. Except where indicated otherwise, the temperature is maintained near a fixed value via the method of Berendsen *et al.* [26] using a time constant of $\tau_T = 0.5$ ps.
[25] O. Steinhauser, Mol. Phys. **45**, 335 (1982).
[26] H. J. C. Berendsen, J. P. M. Postma, W. F. van Gunsteren, A. DiNola, and J. R. Haak, J. Chem. Phys. **81**, 3684 (1984).
[27] The transition from ice I_h to HDA ice was reproduced in computer simulations by J. S. Tse and M. L. Klein, Phys. Rev. Lett. **58**, 1672 (1987); J. Chem. Phys. **92**, 3992 (1990). Their success is a principal motivation for the present work.
[28] F. H. Stillinger and A. Rahman, J. Chem. Phys. **60**, 1545 (1974).
[29] W. L. Jorgensen, J. Chandrasekhar, J. Madura, R. W. Impey, and M. Klein, J. Chem. Phys. **79**, 926 (1983).
[30] The liquid state configurations are obtained, for ST2, from a 725-ps run at $T = 250$ K and $\rho = 0.87$ g/cm^3; and for TIP4P from a 1794 ps run at $T = 250$ K and $\rho = 0.90$ g/cm^3. The resulting equilibrated configurations are then used to initiate a 180-ps run in which $T = 200$ K (with $\tau_T = 2.0$ ps) in the temperature control. In this way the initially liquid system is cooled to an amorphous solid state at $T = 200$ K. This amorphous solid configuration is then itself subjected to a similar period of cooling over 50 ps to bring T into the range in which amorphous solid water is observed; this second stage of cooling is carried out three separate times to produce distinct amorphous solid states at $T = 180$, 130, and 80 K.
[31] The isothermal compression is carried out via a MD simulation in which the value of P to which the simulation is constrained (again, using the method of Berendsen, *et. al.* [26]) is stepwise increased by $\Delta P = 25$ MPa every $\Delta t = 10$ ps. The average density of the system during each 10-ps interval is calculated, yielding the pressure-density relationship for the given T. Checks of some of the resulting compression isotherms using $\Delta P = 50$ MPa and $\Delta t = 10$ ps, and using $\Delta P = 25$ MPa and $\Delta t = 20$ ps do not give significantly different results.

[32] P. H. Poole, F. Sciortino, U. Essmann, and H. E. Stanley, Nature **360**, 324 (1992); Phys. Rev. E **48**, 3799 (1993).
[33] P. H. Poole, Ph.D. thesis, Boston University (1993).
[34] M. R. Chowdhury, J. C. Dore, and J. T. Wenzel, J. Non-Cryst. Sol. **53**, 247 (1982).
[35] A. Bizid, L. Bosio, A. Defrain, and M. Oumezzine, J. Chem. Phys. **87**, 2225 (1987).
[36] M.-C. Bellissent-Funel, J. Teixeira, and L. Bosio, J. Chem. Phys. **87**, 2231 (1987).
[37] M.-C. Bellissent-Funel, J. Teixeira, L. Bosio, and J. C. Dore, J. Phys. Condens. Matter **1**, 7123 (1989).
[38] The $h(r)$ function can be calculated from the pair correlation functions $g_{\mathrm{O-O}}(r)$, $g_{\mathrm{O-H}}(r)$ and $g_{\mathrm{H-H}}(r)$, which give the probabilities of an atom of a particular type to be in a differential radial distance element dr at a distance r from a given atom; here, O refers to oxygen atoms, and H to hydrogen atoms. In a neutron-scattering study of water, a weighted sum $h(r)$ of these radial distribution functions can be calculated [34], and is given by $h(r) = 4\pi\rho r[0.092g_{\mathrm{O-O}}(r) + 0.422g_{\mathrm{O-H}}(r) + 0.486g_{\mathrm{H-H}}(r) - 1]$.